JCTC Journal of Chemical Theory and Computation

Article

pubs.acs.org/JCTC

A Glycam-Based Force Field for Simulations of Lipopolysaccharide Membranes: Parametrization and Validation

Karl N. Kirschner,*[,†] Roberto D. Lins,[§] Astrid Maass,[‡] and Thereza A. Soares*[,§]

[†]Fraunhofer-Institute for Algorithms and Scientific Computing (SCAI), Department of Bioinformatics, Schloss Birlinghoven, 53754 Sankt Augustin, Germany

[‡]Fraunhofer-Institute for Algorithms and Scientific Computing (SCAI), Department of Simulation Engineering, Schloss Birlinghoven, 53754 Sankt Augustin, Germany

[§]Department of Fundamental Chemistry, Federal University of Pernambuco, Cidade Universitária, Recife, PE 50740-560 Brazil

Supporting Information

ABSTRACT: Lipopolysaccharides (LPS) comprise the outermost layer of the Gram-negative bacteria cell envelope. Packed onto a lipid layer, the outer membrane displays remarkable physical−chemical differences compared to cell membranes. The carbohydrate-rich region confers a membrane asymmetry that underlies many biological processes such as endotoxicity, antibiotic resistance, and cell adhesion. Furthermore, unlike membrane proteins from other sources, integral outer-membrane proteins do not consist of transmembrane α helices; instead they consist of antiparallel β-barrels, which highlights the importance of the LPS membrane as a medium. In this work, we present an extension of the GLYCAM06 force field that has been specifically developed for LPS membranes using our Wolf$_2$Pack program. This new set of parameters for lipopolysaccharide molecules expands the GLYCAM06 repertoire of monosaccharides to include phosphorylated *N*- and *O*-acetylglucosamine, 3-deoxy-D-*manno*-oct-2-ulosonic acid, L-glycero-D-*manno*-heptose and its O-carbamoylated variant, and *N*-alanine-D-galactosamine. A total of 1 μs of molecular dynamics simulations of the rough LPS membrane of *Pseudomonas aeruginosa* PA01 is used to showcase the added parameter set. The equilibration of the LPS membrane is shown to be significantly slower compared to phospholipid membranes, on the order of 500 ns. It is further shown that water molecules penetrate the hydrocarbon region up to the terminal methyl groups, much deeper than commonly observed for phospholipid bilayers, and in agreement with neutron diffraction measurements. A comparison of simulated structural, dynamical, and electrostatic properties against corresponding experimentally available data shows that the present parameter set reproduces well the overall structure and the permeability of LPS membranes in the liquid-crystalline phase.

1. INTRODUCTION

The cell envelope of Gram-negative bacteria consists of a cytoplasmic membrane, a peptidoglycan layer, and an outer membrane. Whereas the inner membrane is exclusively composed of phospholipids in a bilayer arrangement, the outer membrane is strictly asymmetric with respect to its lipid composition and electrostatic potential. It consists of a phospholipid inner leaflet and a lipopolysaccharide (LPS) outer leaflet. LPSs from different species have a common general architecture with three distinct regions (Figure 1).[1] Lipid-A consists of two glucosamine−phosphate moieties bound to lipid chains that can vary in length and number depending on the bacterial strain. Lipid-A is the endotoxically active part of the molecule. Covalently linked to Lipid-A is a core oligosaccharide that can be divided into an inner- and outer-core region. The inner core contains a high proportion of the 3-deoxy-D-manno-octulosonic acid (KDO) and L-glycero-D-manno-heptose (HEP), whereas the outer core consists of common sugars such as hexoses and hexamines. Onto this, a polymer of repeating saccharide subunits called O-antigen is attached. These oligosaccharides, typically hexoses, determine the serotype specificity of LPS molecules. The O-antigen region is often truncated or missing in particular strains.[1] The core oligosaccharide of LPS is negatively charged, resulting in a strong affinity for divalent cations.[2] *Pseudomonas aeruginosa* is among the Gram-negative bacteria with the most highly phosphorylated saccharides in the inner core region, with three phosphate groups on the C2, C4, and C6 positions of the inner core heptose.[3,4] These, together with the phosphate groups on both proximal and distal glucosamine head groups of Lipid-A are essential for the integrity of the membrane through strong ionic interactions between the negatively charged core oligosaccharide and divalent counterions.[4]

The resulting network of divalent cations and LPS forms a strong permeability barrier to hydrophilic and hydrophobic compounds, and in which outer membrane proteins are inserted to facilitate the influx of nutrients and also to expel xenobiotic compounds.[5−7] In part due to the unique molecular architecture of the outer membrane, efflux-mediated antibiotic resistance is a more complex problem in Gram-negative than in Gram-positive bacteria.[8] Often drug resistance is attributable to synergy between reduced drug intake (mainly due to low outer-membrane permeability) and active drug export (via efflux pumps).[7,8] *P. aeruginosa* has also a notoriously high intrinsic drug resistance resulting from the synergy between an exceptionally low outer-membrane permeability (approximately 8% of that of *E. coli*) and the presence of specific outer-

Received: June 25, 2012
Published: August 28, 2012

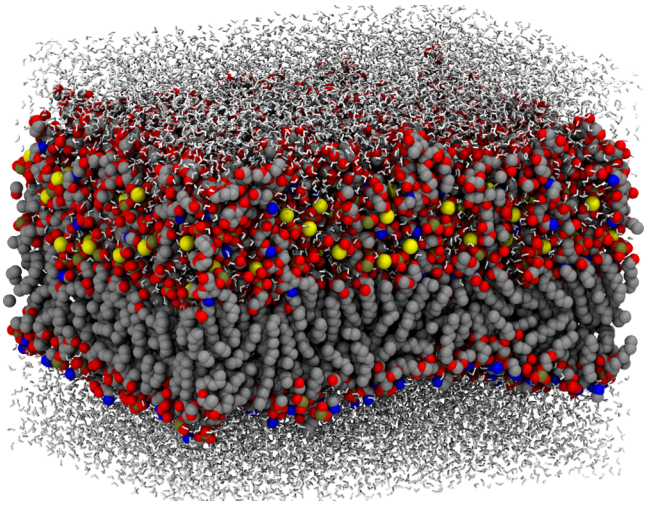

Figure 1. Molecular representation of the LPS-DPPE bilayer. Bilayer atoms are represented by balls (gray for carbon, red for oxygen, blue for nitrogen, yellow for Ca^{2+}) and water molecules by sticks (white).

membrane proteins.[9,10] On that account, *P. aeruginosa* is susceptible only to a few representatives of three classes of antibiotics (fluoroquinolones, beta-lactams, and aminoglycosides) out of all approved antibiotics (ca. 160 antibiotics).[5] Furthermore, the outer-membrane asymmetry resulting from the presence of the LPS leaflet has been shown to play an important role in the electrostatic properties of outer-membrane proteins and low permeability of Gram-negative bacteria.[7,11−15]

Improving the atomistic understanding of the outer-membrane physical−chemical properties enables researchers to design new experiments and compounds that can target the LPS molecular and supra-molecular structures.[16−18] Toward this goal, computational simulation is a powerful tool that can provide structural, dynamical, and thermodynamical information on such systems.[19−22] Current MD simulations can offer an accurate representation of the physical behavior of lipid bilayers ranging from fully atomistic,[23−28] to united atom,[29−33] to mesoscale resolutions.[34−36] In the past decade, there has been a continuous effort to model LPS membranes at the atomistic level.[37−43] The first computational simulation of a LPS membrane was performed with a generic adaptation of the AMBER96[44] and the GLYCAM93[45] force fields to represent the lipid and carbohydrate molecules, respectively.[37] These parameters were subsequently tested via several simulations of the rough[37,41] and smooth (rough LPS + O-antigen)[39] LPS membranes from *P. aeruginosa* and applied to the simulation of an outer-membrane protein embedded in a LPS membrane.[40,42] More recently, atomistic parameters for the Lipid-A portion of the LPS from *P. aeruginosa*[46] and the shorter LPS chemotype Rd1 (Lipid-A + inner core) from *Escherichia coli*[47] compatible with the GROMOS force field have also become available.

The GLYCAM force field[48] has come across several developments from the original parameter set used in the previous LPS membrane simulations as higher-quality experimental data became available and computer power increased to allow force field parameters to be tested and improved.[21,22,49−52] The GLYCAM06 parameter set departed from using 1−4 nonbonded scaling factors and assignment of

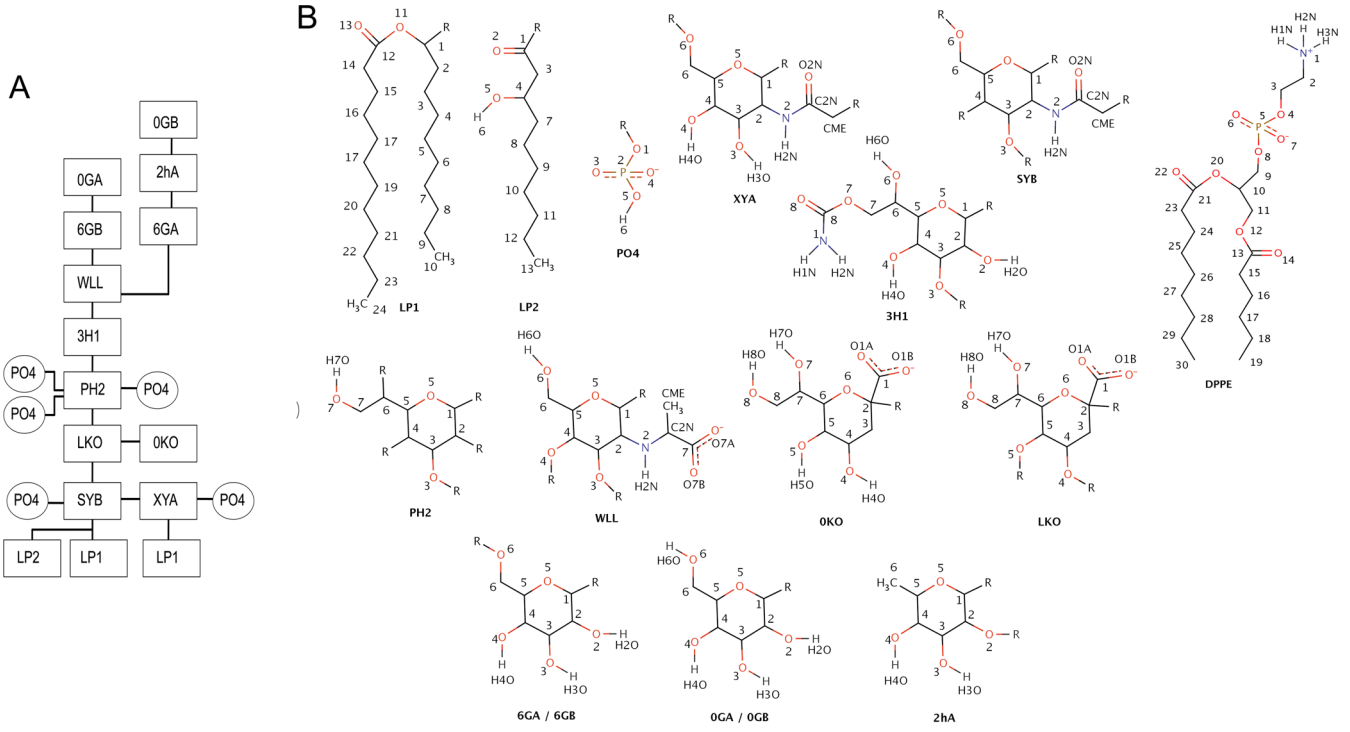

Figure 2. Schematic representation of one unit of the PA01 LPS chemotype from *Pseudomonas aeruginosa* (A) and the chemical structure of the LPS constituent building blocks (B). Residue names stand for 6-α-D-glucose (6GA), 0-β-D-glucose (0GB), 2-α-L-rhamnose (2hA), 3-(*acetyl amino*)-3-deoxy-D-glucose (XYB and variant SYB), 3-deoxy-D-*manno*-oct-2-ulosonic acid (0KO and variant LKO), L-glycero-D-*manno*-heptose-7-formamide (3H1), 2-(2-hydroxyethyl)-6-deoxy-D-*manno*-heptose (PH2), 2-(2-L-alanyl)-2-deoxy-D-galactosamine (WLL), dodecanoyl acid (12:0) (LP1), and 3-hydroxydecanoyl acid 10:0 (3-OH) (LP2). Residues 6GB, 0GA, and 2hA are already available in the GLYCAM06 distribution.

dx.doi.org/10.1021/ct300534j | J. Chem. Theory Comput. 2012, 8, 4719−4731

partial charges to every atom; instead the QM molecular electrostatic potentials were obtained by not fitting partial charges to aliphatic hydrogens. The latest GLYCAM06 in conjunction with the PARM94[53] parameter set for van der Waals tackled some critical limitations of the GLYCAM95 set such as poor reproduction of diffusion rates in explicit solvent and solvation behavior.[48]

Currently available carbohydrate parameters for LPS and its chemotypes have been built via assignment by analogy to pre-existing force field parameters.[38,47] Indeed, the GROMOS[54,55] and GLYCAM[48] force fields have parameters for the common hexoses and hexamines found in the outer-core region of the LPS molecule (Figure 2A). However, the LPS inner core contains a high proportion of unusual carbohydrates for which force field parameters are not readily available. The diverse chemical composition, and the resulting differences in the chirality and chemical substituents of monosaccharides, may lead to rather distinct conformational preferences for dihedrals and puckering angles. In such cases, transferability of parameters should be taken with caution.[56−58] We have addressed this point by developing a new set of parameters for lipopolysaccharide molecules, which expands the GLYCAM06 repertoire of monosaccharides to include phosphorylated *N*- and *O*-acetylglucosamine, 3-deoxy-D-*manno*-oct-2-ulosonic acid, L-glycero-D-*manno*-heptose and its O-carbamoylated variant, and *N*-alanine-D-galactosamine. Herein, we report on the development and validation of these parameters using the rough PA01 LPS chemotype from *P. aeruginosa* on top of a 1,2-dipalmitoyl-3-phosphatidyl-ethanolamine (DPPE) lipid layer as our showcase. Parameter validation for the liquid-crystalline phase is presented for MD simulations at 300 K and 350 K for a total of 1 μs against a variety of available experimental data. For parameter availability, see the Supporting Information.

2. METHODOLOGY

2.1. Parameterization. GLYCAM06 provided the partial atomic charges for residues in the outer core (0GA, 0GB, 6GA, 6GB, and 2hA) and many of the parameters necessary for simulation (Figure 2). However, several additional residues (LP1, LP2, PO4, 3H1, 0KO, WLL, XYA, LKO, PH2, and SYB) and parameters required model building and optimization since they were not available at the start of this research (Figure 2). These residue names stand for 6-α-D-glucose (6GB), 0-β-D-glucose (0GA), 2-α-L-rhamnose (2hA), 3-(*acetyl amino*)-3-deoxy-D-glucose (XYB and variant SYB), 3-deoxy-D-*manno*-oct-2-ulosonic acid (0KO and variant LKO), L-glycero-D-*manno*-heptose-7-formamide (3H1), 2-(2-hydroxyethyl)-6-deoxy-D-*manno*-heptose (PH2), 2-(2-L-alanyl)-2-deoxy-D-galactosamine (WLL), dodecanoyl acid (12:0) (LP1), and 3-hydroxydecanoyl acid 10:0 (3-OH) (LP2). It should be noticed that distinct acylation patterns of Lipid-A can be easily built by adding or removing the residue LP2.

All initial structures were created using PyMOL[59] saved as a PDB file and converted to the GAMESS-US[60] format using openBabel.[61] All geometry optimizations were performed using the restricted closed-shell Hartree−Fock (HF) with a 6-31G(d) basis set. Stationary point characterizations were done by performing frequency analyses; projected Hessian matrices were computed using an analytical method. For creation of the potential energy curves, constrained optimizations were performed by specifying an internal coordinate to be frozen while all other degrees of freedom were allowed to relax fully. Subsequent single self-consistent field calculations were also performed using the Becke three parameter Lee−Yang−Parr hybrid density function (B3LYP) using the 6-311++G(2d,2p) basis set. This method was chosen to be consistent with GLYCAM06's force field development.[48]

RESP-derived partial atomic charges[44,62] were computed for each training molecule by fitting to the HF/aug-cc-pVDZ molecular electrostatic potentials (MEPs). MEPs were computed using the CHELPG methodology[63] with a 0.3 Å point spacing. An SCF convergence criterion of 1.0×10^{-6} was used for all calculations. Multiple molecular orientations were used to compute each MEP.[63,64] A restraint weight of 0.0005 was used in the RESP calculations, and partial atomic charges on the aliphatic hydrogens were constrained to zero during the fitting in order to be compatible with GLYCAM06. RESP-derived partial atomic charges were computed by fitting to a single HF/6-31G(d) MEP (i.e., without multiple molecular orientations) with a restraint weight of 0.01. This is the same level of theory and restraint weight used for developing GYCAM06 residues.[48] All MEP and RESP calculations were performed with the aid of the RED III algorithm.[65]

The AMBER potential energy functional form was used in all molecular mechanics (MM) optimization.[66] Scaling factors for 1−4 nonbonded and electrostatic interactions were set to unity, for reasons previously discussed.[48] The torsion phase angles were constrained to zero, since they are generally unnecessary for fitting torsion profiles. The nonbonded cutoff radius was set to 100 Å, which encompasses every molecule's molecular diameter. Lennard-Jones parameters were adopted from GLYCAM06 and Parm99 force fields.[44,48] Relative energetics and geometries were assessed during each optimization cycle until an optimal parameter solution was found that best fits the quantum mechanics (QM) data. Structural root-mean-square deviations (RMSDs) were determined by referencing each constrained molecular-mechanics geometry to the corresponding quantum geometry using the Ptraj program.[67]

The GAMESS-US software was used to perform all QM calculations.[60] The AMBER9 program package was used for all MM calculations.[67] The resulting parameters and models were transferred to GROMACS format.[68] Correct transferal of parameters was validated by performing energy minimizations and comparison to the resulting energy to that obtained by AMBER. $Wolf_2Pack$, a scientific workflow package for force-field optimization, was used to assist us in all parameter optimization.[69] Gnuplot was used to generate the bond stretching, angle bending, and torsion rotational curves.[70]

2.2. Molecular Simulations. The model of the rough LPS molecule was built from the chemical composition information from mass spectroscopy studies.[71,72] The outer membrane fragment of *P. aeruginosa* simulated in this study consisted of monolayers of 72 LPS molecules and 180 DPPE molecules. In order to balance charged functional groups on the saccharide units at pH 7, a total of 3.5 Ca^{2+} ions per LPS are required. The location of these ions in the inner and outer core of the molecule makes the conventional approaches used to construct and equilibrate phospholipids bilayers inadequate for LPS membranes. A multiple-step protocol was previously developed for this purpose[41] and was used here to compact the membrane to a density near the experimental value.[73]

The equilibration procedure consisted of thermalization of the solvent, with the solute atoms fixed for 500 ps at 300 K followed by an increase of the temperature of the entire system from 0 to 300 K via 100 ps increments of 100 K. This system

Table 1. Atom Type, Bond, Angle, and Torsion Parameters Developed for the LPS Molecule of *Pseudomonas aeruginosa*[a]

atom type	R^*	ε	description
C	1.9080	0.0860	C, sp^2 carbonyl
CX	1.9080	0.1094	C, sp^3 aliphatic
CY	1.9080	0.1094	C, sp^3 aliphatic that is used for sialic acid only
H	0.6000	0.0157	H, attached to a nitrogen
H1	1.3870	0.0157	H, attached to a carbon with 1 e^- withdrawing group
H2	1.2870	0.0157	H, attached to a carbon with 2 e^- withdrawing group
HC	1.4870	0.0157	H, attached to a carbon, which is not attached to an e^- withdrawing group
HO	0.0000	0.000	H, attached to an alcohol O
N	1.8240	0.1700	N, amide
N3	1.8240	0.1700	N, sp^3 positively charge
NT	1.8240	0.1700	N, sp^3
O	1.6612	0.2100	O, carbonyl
O2	1.6612	0.2100	O, R-CO_2^-
OH	1.7210	0.2104	O, alcohol
OS	1.6837	0.1700	O, ether
OY	1.6837	0.1700	O, ether that is used for sialic acid only
P	2.1000	0.2000	P, R−O−P(OH)O_2^-

bond parameters	K_l	l_o	bond parameters	K_l	l_o	bond parameters	K_l	l_o
C−CX	330.0	1.500	CX−H1	410.0	1.092	CY−OS[b]	320.0	1.410
C−CY[b]	220.0	1.530	CX−-H2	440.0	1.105	CY−OY[b]	320.0	1.410
C−N	490.0	1.360	CX−HC	360.0	1.095	H−N	600.0	1.010
C−O	999.0	1.204	CX−N[b]	337.0	1.450	H−NT	544.0	1.010
C−O2	730.0	1.260	CX−NT	344.0	1.420	HO−OH	700.0	0.960
C−OS	411.3	1.343	CX−OH[b]	320.0	1.430	O2−P	750.0	1.500
CX−CX[b]	310.0	1.520	CX−OS	320.0	1.410	OH−P	285.0	1.730
CX−CY[b]	310.0	1.520	CX−OY[b]	320.0	1.410	OS−P	260.0	1.675
angle parameters	K_θ	θ_o	angle parameters	K_θ	θ_o	angle parameters	K_θ	θ_o
CX−C−N[b]	70.0	115.6	CX−CX−NT	60.0	114.5	OS−CY−OY[b]	100.0	112.0
CX−C−O	59.0	125.4	CX−CX−OH[b]	70.0	107.5	C−N−CX[b]	50.0	120.0
CX−C−O2[b]	70.0	115.0	CX−CX−OS[b]	70.0	108.5	C−N−H	50.0	120.5
CX−C−OS	50.0	111.0	CX−CX−OY[b]	70.0	108.5	CX−N−H[b]	30.0	118.0
CY−C−O2[b]	70.0	115.0	CY−CX−HC[b]	45.0	112.6	H−N−H	30.0	108.0
N−C−O	80.0	130.0	H1−CX−H1[b]	45.0	109.5	CX−NT−CX	50.0	109.5
N−C−OS	110.0	114.0	H1−CX−N[b]	50.0	109.5	CX−NT−H	50.0	109.5
O−C−OS	103.0	122.5	H1−CX−NT	45.0	112.5	CX−OH−HO[b]	55.0	109.5
O2−C−O2	100.0	130.0	H1−CX−OH[b]	60.0	110.0	HO−OH−P	54.0	118.5
C−CX−CX	40.0	111.5	H1−CX−OS[b]	60.0	110.0	C−OS−CX	50.6	114.0
C−CX−H1	60.0	108.5	H1−CX−OY[b]	60.0	110.0	CX−OS−CX	50.0	108.5
C−CX−HC	37.0	110.0	H2−CX−OS[b]	60.0	110.0	CX−OS−CY[b]	50.0	111.5
bond parameters	K_l	l_o	bond parameters	K_l	l_o	bond parameters	K_l	l_o
C−CX−NT	60.0	100.0	HC−CX−HC[b]	40.0	109.5	CX−OS−P	35.0	116.0
CX−CX−CX[b]	45.0	113.5	OS−CX−OS[b]	100.0	112.0	CX−OY−CY[b]	50.0	111.6
CX−CX−CY[b]	45.0	113.5	C−CY−CX[b]	63.0	111.1	O2−P−O2	80.0	122.0
CX−CX−H1[b]	45.0	111.0	C−CY−OS[b]	63.0	112.4	O2−P−OH	90.0	108.5
CX−CX−H2[b]	45.0	111.0	C−CY−OY[b]	63.0	112.4	O2−P−OS	101.0	103.5
CX−CX−HC[b]	45.0	112.6	CX−CY−OS[b]	70.0	108.5	OH−P−OS	80.0	100.0
CX−CX−N[b]	80.0	109.7	CX−CY−OY[b]	70.0	108.5			

torsion definition	V_1	V_2	V_3	torsion definition	V_1	V_2	V_3
N−C−CX−CX[b]	0.05	−0.70	0.20	HC−CX−CX−OH[b]			0.05
N−C−CX−HC[b]			0.00	HC−CX−CX−OS[b]			0.05
O−C−CX−CX		−0.41	−0.29	N−CX−CX−OH[b]	−1.50		
O−C−CX−HC			−0.10	N−CX−CX−OS[b]	−1.30		
O2−C −CX−CX[b]	0.01	−0.82	0.02	NT−CX−CX−OS	−0.90		
O2−C −CX−H1[b]			0.00	OH−CX−CX−OH[b]	−0.10	0.95	0.55
O2−C −CX−NT		−0.60		OH−CX−CX−OS[b]	−1.10	0.25	
OS−C −CX−CX		−0.45	−0.33	OH−CX−CX−OY[b]	−1.10	0.25	
OS−C −CX−HC			−0.12	OS−CX−CX−OS[b]		0.82	
O2−C −CY−CX[b]		−1.50		OS−CX−CX−OY[b]		0.82	
O2−C −CY−OS[b]		−2.25		CX−CX−CY−C[b]			0.45
O2−C −CY−OY[b]		−2.25		CX−CX−CY−OS[b]	−0.27		

dx.doi.org/10.1021/ct300534j | J. Chem. Theory Comput. 2012, 8, 4719−4731

Table 1. continued

torsion definition	V_1	V_2	V_3	torsion definition	V_1	V_2	V_3
CX−C −N−CX[b]		−2.70		CX−CX−CY−OY[b]	−0.27		
CX−C−N−H[b]			0.00	HC−CX−CY−C[b]			0.10
O−C−N−CX[b]		−2.80		HC−CX−CY−OS[b]			0.05
O−C−N−H[b]	2.00	−2.50		HC−CX−CY−OY[b]			0.05
OS−C −N−H		−1.50		CX−CX−N−C[b]			0.00
CX−C−OS−CX	−0.65	−2.75		CX−CX−N−H[b]			0.10
N−C−OS−CX	−1.70	−2.60		H1−CX−N−C[b]	−1.00		
O−C−OS−CX		−4.21	−0.73	H1−CX−N−H[b]	1.00		
C−CX−CX−CX			0.00	C−CX−NT−CX	0.50		
C−CX−CX−H1[b]			0.10	C−CX−NT−H		−2.00	
C−CX−CX−HC			−0.03	CX−CX−NT−CX[b]	0.10	−0.20	0.10
C−CX−CX−OH[b]	−2.50	0.20	0.10	CX−CX−NT−H		0.80	
C−CX−CX−OS[b]	−1.00	0.10	−0.10	H1−CX−NT−CX[b]			0.25
CX−CX−CX−CX[b]	0.45			H1−CX−NT−H			0.15
CX−CX−CX−CY[b]	0.45			CX−CX−OH−HO[b]			0.18
CX−CX−CX−H1[b]			0.15	H1−CX−OH−HO[b]			0.18
CX−CX−CX−H2[b]			0.15	CX−CX−OS−C[b]	0.47		−0.04
CX−CX−CX−HC[b]			0.10	CX−CX−OS−CX[b]			0.16
CX−CX−CX−N[b]	0.40			CX−CX−OS−CY[b]			0.16
CX−CX−CX−NT			0.20	CX−CX−OS−P	−1.50		0.15
CX−CX−CX−OH[b]			0.10	H1−CX−OS−C			−0.15
CX−CX−CX−OS[b]	−0.27			H1−CX−OS−CX[b]			0.27
CX−CX−CX−OY[b]	−0.27			H1−CX−OS−CY[b]			0.27
CY−CX−CX−H1[b]			0.15	H1−CX−OS−P	0.05		
CY−CX−CX−OH[b]			0.10	H2−CX−OS−CX[b]		0.60	0.10
CY−CX−CX−OS[b]	−0.27			H2−CX−OS−P			0.10
H1−CX−CX−H1[b]			0.17	OS−CX−OS−CX[b]	0.30	1.27	0.37
H1−CX−CX−H2[b]			0.17	OS−CX−OS−P	−2.57		−0.30
H1−CX−CX−HC[b]			0.17	CX−CX−OY−CY[b]			0.16
H1−CX−CX−N[b]			0.10	H1−CX−OY−CY[b]			0.27
H1−CX−CX−NT			0.15	C −CY−OS−CX[b]	3.50		
H1−CX−CX−OH[b]			0.05	CX−CY−OS−CX[b]			0.16
H1−CX−CX−OS			0.10	OY−CY−OS−CX[b]	0.30	1.27	0.37
H1−CX−CX−OY[b]			0.05	C −CY−OY−CX[b]			0.00
H2−CX−CX−N[b]			0.10	CX−CY−OY−CX[b]			0.16
H2−CX−CX−NT			0.15	OS−CY−OY−CX[b]	0.30	1.27	0.37
H2−CX−CX−OH[b]			0.05	HO−OH−P−O2		−0.25	
H2−CX−CX−OS[b]			0.05	HO−OH−P−OS		0.30	
HC−CX−CX−HC[b]			0.13	CX−OS−P−O2		−0.30	0.35
HC−CX−CX−NT[b]			0.10	CX−OS−P −OH		0.60	−0.25

[a]Bond stretching, angle bending, and torsion rotation constants are in kcal·mol^{-1}·Å^{-2}, kcal·mol^{-1}·rad^{-2}, and kcal·mol^{-1}, respectively. The nonbonded parameters R^* and ϵ are given in Å and kcal·mol^{-1}, which were taken from Cornell et al.[53] For QM-fitted dihedral rotational profiles, see the Supporting Information. [b]Originally derived for GLYCAM06,[49] or taken from Glycam_06g-1,[98] for which the CG atom was used for sp^3 carbon atoms.

was simulated for ca. 500 ns at 300 K. The structure corresponding to the frame at 490 ns of simulation was subsequently used as the starting conformation for the simulation at 350 K. We have chosen to improve sampling by increasing the temperature of the system. This choice was motivated by the long time length required to equilibrate the LPS-DPPE bilayer, and the fact that such a temperature increase does not result in any phase transition. Both temperatures are within and above the gel to liquid-crystalline transition temperatures observed for LPS membranes from *P. aeruginosa*, which is in the range of 303−313 K.[74,75] Periodic boundary conditions were applied to the system based on a rectangular box containing the hydrated LPS-DPPE bilayer in the *xy* plane, i.e., normal to the *z* axis. The TIP3P water model was used to describe solvent atoms for its standard use with the AMBER and GLYCAM force fields.[76] Simulations were performed in the isothermal−isobaric ensemble (NPT) with a time step of 2 fs, and in the absence of any artificial external surface tension parameter. The center of mass motion was removed every five steps. Temperatures of the solute and solvent degrees of freedom were separately coupled to a Berendsen thermostat[77] at 300 K with a relaxation time of 0.2 ps. The pressure was maintained by weakly coupling[77] the particle coordinates and box dimensions in the *xy* plane and along the *z* axis separately to a pressure bath at 1.0 bar by means of semi-isotropic coordinate scaling with a relaxation time of 0.4 ps and a compressibility of 4.5×10^{-5} (kJ mol^{-1} nm^{-3})$^{-1}$ as appropriate for water. Bond lengths between hydrogen and heavy atoms and the geometry of the water molecules were constrained using the linear constraint solver algorithm with a tolerance of 10^{-4}.[78] A reaction field correction and a cutoff of 1.4 nm was used for both vdW and long-range

Table 2. Atom Label, Types, and Partial Atomic Charges for the Residues Generated for Use in Gram-Negative Bacterial Lipids[a]

LP1		LP2		3H1		SYB	
atom (type)	partial atomic charge	atom (type)	partial atomic charge	atom (type)	partial atomic charge	atom (type)	partial atomic charge
C_1 (CX)	0.3849	C_1 (CX)	0.3762	C_1 (CX)	0.3970	C_1 (CX)	0.2870
C_2 (CX)	−0.1481	O_2 (O)	−0.4491	C_2 (CX)	0.3121	C_2 (CX)	0.4800
C_3 (CX)	0.0186	C_3 (CX)	0.0447	O_2 (OH)	−0.6770	N_2 (N2)	−0.7220
C_4 (CX)	0.0793	C_4 (CX)	0.2205	H_{H2O} (HO)	0.3852	H_{H2N} (H)	0.3000
C_5 (CX)	−0.0212	O_5 (OH)	−0.5219	C_3 (CX)	0.3554	C_{C2N} (C)	0.6480
C_6 (CX)	−0.0260	H_6 (HO)	0.2950	O_3 (OH)	−0.4841	C_{O2N} (O)	−0.5760
C_7 (CX)	0.0113	C_7 (CX)	0.0398	C_4 (CX)	0.1583	C_{CME} (CX)	0.0340
C_8 (CX)	0.0140	C_8 (CX)	−0.0128	O_4 (OH)	−0.7185	C_3 (CX)	0.1800
C_9 (CX)	0.0060	C_9 (CX)	0.0067	H_{H4O} (HO)	0.4585	O_3 (OS)	−0.5380
C_{10} (CX)	−0.0096	C_{10} (CX)	−0.0024	C_5 (CX)	0.2689	C_4 (CX)	0.3020
O_{11} (OS)	−0.4676	C_{11} (CX)	0.0112	O_5 (OS)	−0.5190	C_5 (CX)	0.2080
C_{12} (CX)	0.6503	C_{12} (CX)	0.0126	C_6 (CX)	0.4606	O_5 (OS)	−0.5330
O_{13} (O)	−0.5419	C_{13} (CX)	−0.0205	O_6 (OH)	−0.7055	C_6 (CX)	0.2890
C_{14} (CX)	0.0498			H_{H6O} (HO)	0.3781	O_6 (OS)	−0.5530
C_{15} (CX)	0.0759			C_7 (CX)	0.2441		
C_{16} (CX)	−0.1481	PO4		O_7 (OS)	−0.5484		
C_{17} (CX)	0.0186	O_1 (OS)	−0.4564	C_8 (C)	1.0884		
C_{18} (CX)	0.0793	P_2 (P)	1.3528	O_8 (O)	−0.6739		
C_{19} (CX)	−0.0212	O_3 (O2)	−0.8002	N_1 (N)	−1.0302		
C_{20} (CX)	−0.0260	O_4 (O2)	−0.8002	H_{H1N} (H)	0.4250		
C_{21} (CX)	0.0113	O_5 (OH)	−0.6915	H_{H2N} (H)	0.4250		
C_{22} (CX)	0.0140	H_6 (HO)	0.3955				
C_{23} (CX)	0.0060						
C_{24} (CX)	−0.0096						

0KO		WLL		XYA		LKO		PH2	
atom (type)	partial atomic charge	atom (type)	partial atomic charge	atom (type)	partial atomic charge	atom (type)	partial atomic charge	atom (type)	partial atomic charge
C_1 (C)	0.7323	C_1 (CX)	0.2055	C_1 (CX)	0.4680	C_1 (C)	0.7323	C_1 (CX)	0.2218
O_{O1A} (O2)	−0.7635	C_2 (CX)	0.0590	C_2 (CX)	0.2450	O_{O1A} (O2)	−0.7635	C_2 (CX)	0.0069
O_{O1B} (O2)	−0.7635	N_2 (NT)	−0.3236	N_2 (N2)	−0.5520	O_{O1B} (O2)	−0.7635	C_3 (CX)	0.3669
C_2 (CX)	0.4349	H_{H2N} (H)	0.1653	H_{H2N} (H)	0.2360	C_2 (CX)	0.4349	O_3 (OS)	−0.4590
C_3 (CX)	−0.0548	C_{C2N} (CX)	0.0824	C_{C2N} (C)	0.5880	C_3 (CX)	−0.0548	C_4 (CX)	0.0405
C_4 (CX)	0.3784	C_{CME} (CX)	−0.0523	C_{O2N} (O)	−0.5790	C_4 (CX)	0.3784	C_5 (CX)	0.3429
O_4 (OH)	−0.7169	C_7 (C)	0.3000	C_{CME} (CX)	0.0630	O_4 (OS)	−0.5128	O_5 (OS)	−0.5780
H_{H4O} (HO)	0.4044	O_{O7A} (O2)	−0.2458	C_3 (CX)	0.1650	C_5 (CX)	0.2028	C_6 (CX)	0.1730
C_5 (CX)	0.2028	O_{O7B} (O2)	−0.2458	O_3 (OH)	−0.6300	O_5 (OS)	−0.4295	C_7 (CX)	0.1534
O_5 (OH)	−0.6165	C_3 (CX)	0.0644	H_{H3O} (HO)	0.4130	C_6 (CX)	0.0585	O_7 (OH)	−0.7295
H_{H5O} (HO)	0.3747	O_3 (OS)	−0.4344	C_4 (CX)	0.3220	O_6 (OS)	−0.5113	H_{H7O} (HO)	0.4611
C_6 (CX)	0.0585	C_4 (CX)	0.0714	O_4 (OH)	−0.7330	C_7 (CX)	0.3186		
O_6 (OS)	−0.5113	O_4 (OS)	−0.4335	H_{H4O} (HO)	0.4490	O_7 (OH)	−0.7474		
C_7 (CX)	0.3186	C_5 (CX)	0.0845	C_5 (CX)	0.2460	H_{H7O} (HO)	0.4614		
O_7 (OH)	−0.7474	O_5 (OS)	−0.3505	O_5 (OS)	−0.5680	C_8 (CX)	0.3153		
H_{H7O} (HO)	0.4614	C_6 (CX)	0.0277	C_6 (CX)	0.3280	O_8 (OH)	−0.7007		
C_8 (CX)	0.3153	O_6 (OH)	−0.4407	O_6 (OS)	−0.4610	H_{H8O} (HO)	0.3873		
O_8 (OH)	−0.7007	H_{H6O} (HO)	0.2724						
H_{H8O} (HO)	0.3873								

[a]Atom labels correspond to Figure 2. Aliphatic hydrogen atoms are not included since their partial atomic charges are zero and their atom type assignment is trivially done.

Table 3. Atom Label, Types, and Partial Atomic Charges for the Residues Generated for Use in the DPPE Lipid[a]

atom (type)	partial atomic charge	atom (type)	partial atomic charge	atom (type)	partial atomic charge	atom (type)	partial atomic charge
N_1 (N3)	−0.0945	O_7 (O2)	−0.7483	C_{15} (CX)	−0.0107	C_{23} (CX)	0.0251
H_{H1N} (H)	0.2272	O_8 (OS)	−0.4721	C_{16} (CX)	−0.0092	C_{24} (CX)	0.0002
H_{H2N} (H)	0.2272	C_9 (CX)	0.1503	C_{17} (CX)	0.0428	C_{25} (CX)	0.0102
H_{H3N} (H)	0.2272	C_{10} (CX)	0.3082	C_{18} (CX)	0.0202	C_{26} (CX)	0.0139
C_2 (CX)	0.1571	C_{11} (CX)	0.2812	C_{19} (CX)	−0.0212	C_{27} (CX)	−0.0257
C_3 (CX)	0.3287	O_{12} (OS)	−0.4462	O_{20} (OS)	−0.4931	C_{28} (CX)	0.0208
O_4 (OS)	−0.5494	C_{13} (C)	0.7525	C_{21} (C)	0.6998	C_{29} (CX)	0.0166
P_5 (P)	1.2869	O_{14} (O)	−0.6028	O_{22} (O)	−0.5545	C_{30} (CX)	−0.0201
O_6 (O2)	−0.7483						

[a]Atom labels correspond to Figure 2. Aliphatic hydrogen atoms are not included since their partial atomic charges are zero and their atom type assignment is trivially done.

electrostatic interactions with a permittivity dielectric constant of 66.[79] In all cases, the pair list for short-range nonbonded and long-range electrostatic interactions was updated with a frequency of five time steps. The LPS membrane was simulated for approximately 500 ns at 300 K and continued to 1.0 μs at 350 K. Configurations of the trajectory were recorded every 2 ps. The software package Gromacs v.4.04 and implemented algorithms were used for all simulations and property analyses.[68,80] Coordinates and trajectories were visualized with the software VMD 1.86.[81]

2.3. Data Analysis. Trajectory analyses were performed for several time windows as well as for the final 500 ns of the simulations at 300 and 350 K. Monitored properties were the area per lipid/LPS molecule; the density distribution of relevant functional groups along the axis normal to the plane of the LPS membrane; the radial distribution function for Ca^{2+} cations, water molecules, carboxylate, and phosphate groups; carbon-deuterium order parameters S_{CD} of lipid tails; and the electrostatic potential across the membrane. The area per lipid/LPS molecule was calculated from the lateral box dimensions divided by the number of lipids/LPS molecules in the corresponding leaflet. Radial distribution functions $g(r)$ were calculated by a histogram summation in radial shells over all molecules in the system. The carbon−deuterium order parameter S_{CD} is defined as

$$S_{CD} = \frac{3}{2}\langle \cos^2 \theta \rangle - \frac{1}{2}$$

where θ is the angle between the carbon−deuterium vector of the ith methylene group in the lipid and the longitudinal axis of the system with the angular brackets denoting ensemble averaging. Order parameters do not only depend on the order−disorder of the system but also on orientation. $S_{CD} = 0$ can be either an unordered (isotropic) system or a perfectly ordered system oriented at the magic angle of 54.7° with respect to the magnetic field. A value of −0.5 indicates a perfectly ordered acyl chain in all-trans conformation, rapidly rotating around the bilayer normal. Deuterium order parameters values are reported here as $|S_{CD}|$.

The difference in electrical potential (voltage) across the LPS membrane was calculated by solving the double integral of the charge density from the trajectories[25]

$$\psi(z) - \psi(-\infty) = -\int_{-\infty}^{z} dz \int_{-\infty}^{z} \rho(z'')\, dz''/\varepsilon_0$$

where ψ is the electrostatic potential across the interface and $\rho(z)$ is the time averaged charge density. The position $z = -\infty$ is assumed to be far enough in the bulk phase so that the field is zero. The system is sliced in layers normal to the Z axis, and the atomic charges across each layer are summed. The electrostatic potential calculations were performed using a total of 100 slices and averaged over 32 600 structures saved at 15 ps intervals throughout 500 ns of simulations.

3. RESULTS AND DISCUSSION

3.1. Parameterization. Within a single lipid molecule (479 atoms) there are 25 unique bond types, 31 unique angle types, and 104 unique dihedral angles. Tables 1 and 2 provide all of the parameters necessary for simulating the LPS studied here, which includes previously published GLYCAM06 parameters. The lipid itself was separated into 20 residues, for which 10 new residues were created within this study (Figure 2). The corresponding atom types and partial atomic charges for each residue are listed in Tables 2 and 3. Aliphatic hydrogens are not listed since their partial atomic charges were set to zero. The atom types HC, H1, and H2 were assigned to the aliphatic hydrogens based on whether their adjoined carbon atoms were bound to zero, one, or two electronegative atoms.

Determining the partial atomic charges for the new residues required a variation of the approach used for developing GLYCAM06. In the development of GLYCAM06, each residue was assigned an overall charge that depended upon the number of connection points it contained. For terminal carbohydrate residues, which contained one connecting point, a noninterger charge of 0.194e was required. For a residue with two connecting points, there was no formal net charge (i.e., 0.0e) required. For residues with three, four, or five connecting points, noninterger charges of −0.194, −0.388, and −0.582e were required. Using this scheme, it is possible to build a branched polysaccharide that is formally neutral, with the initial carbohydrate terminated using a −OCH3 residue whose partial atomic charge is −0.194e. However, Lipid A contains three hydrophobic tail residues, and by the scheme used in developing GLYCAM06, these residues would have assumed a small noninterger formal charge assigned to them. Clearly, if one were to use these residues in constructing the bilayer, an unrealistic electrostatic potential would form within the hydrophobic layer, leading to incorrect membrane behavior during a simulation. In order to avoid that, we required the Lipid-A tail residues (LP1 and LP2) to be overall neutral during the RESP calculations. We subsequently assigned a formal overall charge of −1e to each phosphate residue (PO4), which can be used also for systems that do not contain carbohydrate residues. The remaining LPS residues were assigned overall charges of 0.0e (PH2, XYA, and 3H1), −0.194e (SYB), −0.806e (0KO), and −1.194 e (LKO and WLL). This charge

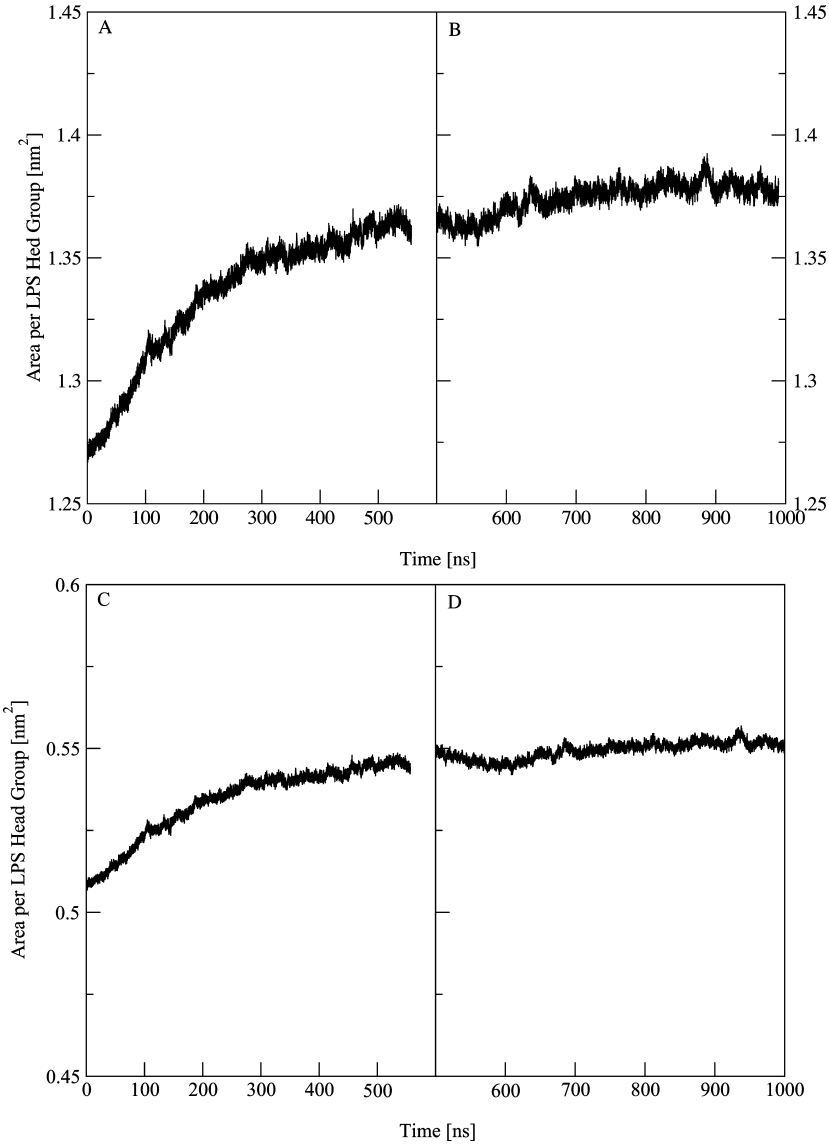

Figure 3. Area per lipid molecule as a function of time for the LPS-DPPE membrane. (A) LPS at 300 K, (B) LPS at 350 K, (C) DPPE at 300, and (D) DPPE at 350 K. The values are averaged over 72 LPS and 180 DPPE molecules, respectively.

assignment scheme results in a LPS that has a −2.194*e* formal charge on Lipid-A, neutral hydrocarbon tails, a −5.0*e* formal charge on the inner core, and a −0.806*e* formal charge on the outer core. Thus, the overall formal charge on the LPS is −7.0*e*. This scheme is a reasonable approach for avoiding artificial charge building within the hydrophobic membrane region, while enabling the use of existing GLYCAM06 residues (0GA, 0GB, 6GB, 2hA, and 6GA).

3.2. Area per Lipid Headgroup. The LPS parameter set was validated via MD simulations of a bilayer comprised of monolayers with 72 LPS molecules and 180 DPPE molecules (Figure 1). These simulations were carried out for about 0.5 μs at 300 K and continued to 1.0 μs at 350 K. Force-field quality was assessed by a comparison of calculated properties such as area per lipid molecule, density profiles, and deuterium order parameters against neutron and X-ray diffraction measurements.

The calculated area per LPS molecule at 300 K averaged around a value of 1.36 nm^2 from 0.3 μs of simulation onward (Figure 3A). After increasing the temperature to 350 K at 0.6 μs, the area per LPS molecule converged to a value of 1.37 nm^2. The experimental estimate of the area per hydrocarbon chain for rough LPS in the liquid-crystalline phase is 0.26 nm^2, which corresponds to 1.3 nm^2 for a pentaacylated LPS molecule.[73] Hence, the calculated value for the area per LPS molecule is within an error of less than 4% of the corresponding experimental value. The area per DPPE molecule at 342 K has been experimentally estimated as 0.55 nm^2, the same average value observed for the simulations at 300 and 350 K.[82]

3.3. Density Profile. The density profile of selected chemical groups across the *Z* axis of the LPS-DPPE bilayer was calculated for the last 100 ns of the simulation (Figure 4). No significant differences were observed for simulations at 300 and 350 K. The central peak corresponds to the hydrocarbon chains from the DPPE and LPS leaflets. It spans a width of 2.1 nm, consistent with the length of two opposing hydrocarbon chains oriented approximately perpendicular to the bilayer plane. There are a total of five phosphate groups per LPS and one per DPPE distributed along three distinct regions of the bilayer (Figure 2). The phosphate group in the DPPE leaflet

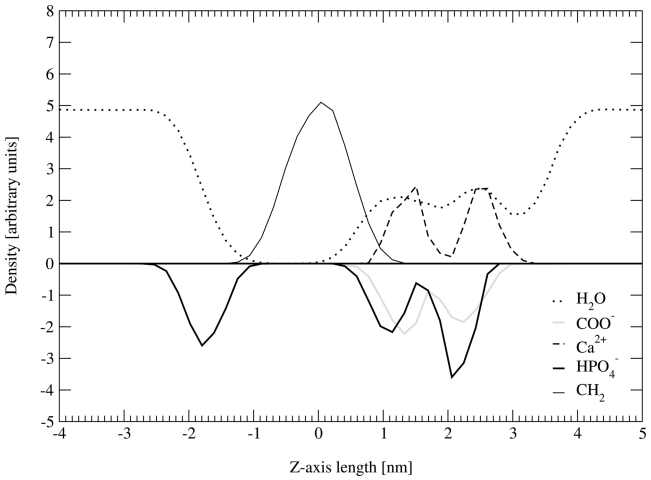

Figure 4. Partial number density along the membrane normal axis of selected chemical groups in the LPS-DPPE bilayer. Partial densities of carboxyl and phosphate groups have their values multiplied by −1 for clarity. The values are averaged over 72 LPS/180 DPPE molecules and over the last 100 ns of simulation.

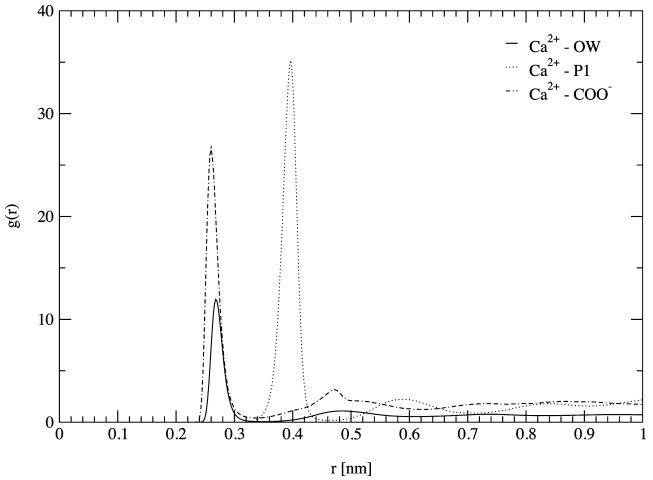

Figure 5. (A) Radial distribution funtion between Ca^{2+} cation and the oxygen atoms in the water molecules (black line), in the phosphate group (dotted line), and in the carbonyl group (dotted-dashed line). Data calculated from simulation at 350 K. No significant difference was observed between simulations at different temperatures. Values are averaged over the final 200 ns of simulations.

corresponds to the peak at 1.8 nm, in line with previous estimates from simulations of pure DPPE bilayers.[83] The two other peaks, one at 1.2 nm and the other at 2.1 nm, represent the phosphate groups of the Lipid-A and inner core portion of the LPS leaflet, respectively (Figure 4). Carboxyl groups occur in the inner core of the LPS molecule near the phosphates groups. In the calculated density profile, these groups are represented by two peaks at 1.3 and 2.3 nm. The peaks at 1.5 and 2.5 nm correspond to Ca^{2+} cations, which were previously shown to bind to the KDO carboxylate groups (k_d = 6 μM) and to the phosphate group (k_d = 56−100 μM) in Lipid-A.[2] Remarkably, the LPS leaflet is highly permeable to the solvent, particularly when compared to the DPPE leaflet (Figure 4). Water molecules penetrate the LPS outward region of the hydrophobic core corresponding to the methylene groups of the Lipid-A. The high permeability of LPS membranes has also been shown by means of neutron scattering measurements obtained for smooth LPS bilayers from *P. aeruginosa* in the liquid-crystalline phase.[74,84] These measurements have shown that water molecules can penetrate the hydrocarbon region up to the terminal methyl groups. Hence, the present GLYCAM-compatible parameter set reproduces the overall structure as well as the permeability of LPS membranes in the liquid-crystalline phase.

3.4. Radial Distribution Function. The radial distribution of water molecules and phosphate and carboxyl groups of the LPS membrane around Ca^{2+} cations located at the inner core and lipid-A regions were calculated for the system at 300 and 350 K. The curves obtained are essentially the same for the two temperatures, and results are presented for the latter. Figure 5 shows three sharp peaks at about 0.26, 0.27, and 0.40 nm, which correspond to the distribution of Ca^{2+} ions around the carboxyl groups in the inner core, the oxygen atom in water molecules, and the phosphorus atom from the phosphate groups in the Lipid-A and the inner core regions of the LPS leaflet, respectively. The high amplitude of the first peak and absence of well-defined secondary peaks in all cases indicates that Ca^{2+} ions bind strongly to the LPS chemical groups but remain partly solvated. Two broader peaks at 4.7 and 5.9 nm are associated with the carboxyl and the phosphate groups, respectively. The integration of the peak area at 0.27 nm shows an average of 3.6 water molecules coordinating the Ca^{2+} cation. The integration of the first peak for the phosphorus atom shows an average of 2.0 phosphate groups interacting with each Ca^{2+} cation at a distance of 0.40 nm. The nearest pair of phosphates belongs to different, though neighboring, LPS molecules. The second pair, with a peak position at 0.59 nm, corresponds to the adjacent phosphate group in each of these two neighboring molecules. The integration of the first peak for the carboxylate group distribution shows that on average it interacts with less than one Ca^{2+} cation (ca. 0.2). These findings indicate that the Ca^{2+} ions bind predominantly to the phosphate groups surrounding the keto-*d*-octulosonic acid (KDO) in a hexa-coordinated geometry, consistently with the experimental literature.[84]

3.5. Deuterium Order Parameters. Deuterium order parameters S_{CD} were calculated for the *sn*-1, *sn*-2, and *sn*-3 acyl chains of the LPS membranes at 300 and 350 K (Figure 6). S_{CD} measures the relative orientation of the C−D bonds with respect to the bilayer normal. Therefore, it functions as a sensor of the degree of order−disorder of acyl chains, which in turn can be associated with their mobility or fluidity (inversely proportional to the state of order). The calculated S_{CD} values are lower than 0.30 for all three acyl chains with increasing disorder along the aliphatic chains toward the methyl groups and decreasing number of carbon atoms (Figure 6). The S_{CD} profile is characteristic of bilayers in the lamellar phase with disordered aliphatic chains.[85−88] Average S_{CD} values for the *sn*-1, *sn*-2, and *sn*-3 acyl chains in the interval between 450 and 600 ns are 0.24, 0.22, and 0.26, respectively. We have also investigated the convergence of the S_{CD} as a function of different time periods along the simulation (Figure 6). The S_{CD} convergence is faster for the shorter aliphatic chain *sn*-3 and for the terminal carbon atoms along all three chains. The orientation of the chain *sn*-3 converged at 300 ns compared to 450 ns for chains *sn*-1 and *sn*-2. Likewise, the S_{CD} for groups at the end of the aliphatic chains reaches full convergence at the aforementioned time scales, whereas the ones in the beginning of these chains exhibit slower dynamics (Figure 6). The

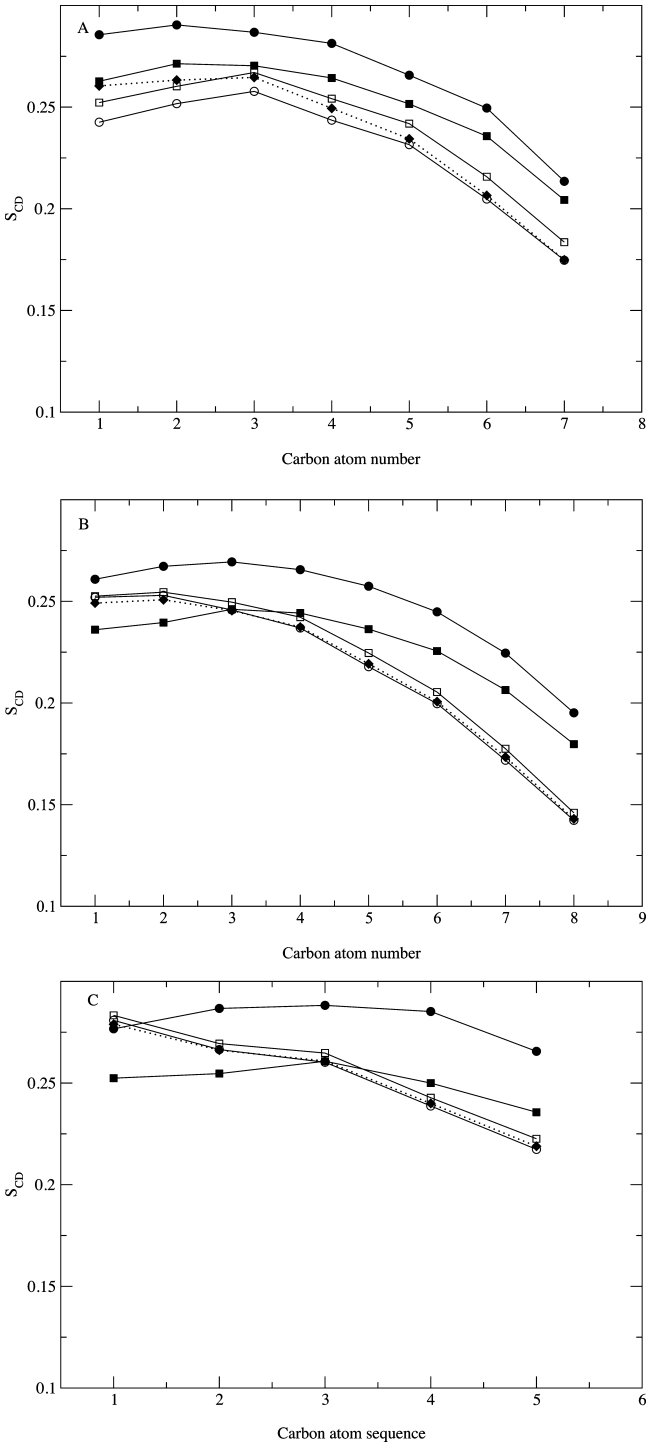

Figure 6. Carbon−deuterium order parameter (S_{CD}) for carbon atoms in the acyl chains of the LPS membrane at 300 K (black line) and 350 K (dotted line). Order parameter values were averaged over 64 LPS molecules and over different time windows: 0−150 ns (filled circle), 150−300 ns (filled square), 300−450 ns (circle), 450−600 ns (square). Values are plotted as a function of the carbon sequence number in acyl chains.

presence of neighboring hydroxyl and carbonyl groups in the *sn*-3 chain may affect the acyl chain packing due to the formation of intramolecular hydrogen bonds and intermolecular interaction with deep penetrating water molecules. It could explain the higher S_{CD} values calculated for acyl groups nearby the hydroxyl group.

Deuterium order parameter S_{CD} values are not available for LPS and Lipid-A membranes. However, attenuated total reflectance measurements coupled to Fourier transform infrared (ATR-FITR) spectroscopy can be used to quantify the molecular orientation of molecules from polarized IR spectra of oriented samples.[89] Hence, an estimate S of the orientational behavior of LPS molecules can be deduced from the peak position x_s of the symmetric stretching vibration of the methylene group around 2850 cm^{-1} via a third order polynomial:[87,88,90,91]

$$S = -941.8 + 0.7217x_s - 7.823 \times 10^{-5}x_s^2 - 2.068 \times 10^{-8}x_s^3$$

Accordingly, S ranges from 1 for perfectly aligned acyl chains to 0 for isotropic systems. A detailed account of the approach applied to LPS membranes is given in ref 87. Typical estimates of S for LPS in the gel and liquid-crystalline phases are 0.70 ± 0.05 (0.80 ± 0.05 for phosphatidylethanolamines) and 0.25 ± 0.05, respectively.[87] The average nature of this measurement does not allow one to distinguish between the orientational behavior of each acyl chain individually. The average S_{CD} calculated over all three acyl chains in the simulations is 0.24 compared to S = 0.28 measured for Lipid-A from *P. aeruginosa* in the liquid-crystalline phase.[75] These order parameters correspond to angle values of 45.4° and 43.9°, i.e., a difference of only 1.5°. The S_{CD} values calculated from the simulations at 300 and 350 K are typical of the liquid-crystalline phase, which is consistent with the calculated area per LPS (Figure 3) and with experimental evidence that the Lα→Lβ transition for the LPS of *P. aeruginosa* starts at temperatures around 303 K.[74,75] MD simulations of a Lipid-A bilayer using the GROMOS force field have also shown the occurrence of a liquid-crystalline phase at similar temperatures.[46]

3.6. Transmembrane Potential. Lipid asymmetry can alter the electric field across the membrane, provoking a potential difference between the two surfaces of the bilayer even in the absence of ion charge gradients across the membrane.[92−95] The simulated bilayer system is representative of the outer membrane of Gram-negative bacteria that consists of an outer leaflet of LPS and an inner leaflet predominantly composed of DPPE.[96,97] Such a bilayer exhibits an extreme asymmetry of charge density between the two leaflet surfaces, which gives rise to an inner membrane potential ranging between −85 mV and −38 mV for the deep rough (LPS Re) mutant of *Escherichia coli* and *Salmonella minnesota*.[15] The structure of the LPS Re chemotype consists of the Lipid-A attached to two KDO units. In *S. minnesota*, the surface potential on the LPS leaflet is ca. −199 mV and on the phospholipid leaflet is −69 mV.[92] The transmembrane potential profile of the simulated LPS membrane was calculated along the axis normal to the bilayer (Figure 7A). The profile was averaged over 32 600 conformations corresponding to the last 500 ns of simulation. The electrostatic potential representing charge distributions along the inner and outer leaflet surfaces was also calculated (Figure 7B). The calculated surface potentials of the LPS and DPPE leaflets are ca. −155 mV and −36 mV, respectively (Figure 7A). The resulting transmembrane potential is ca. −119 mV, and within experimental estimates.[15]

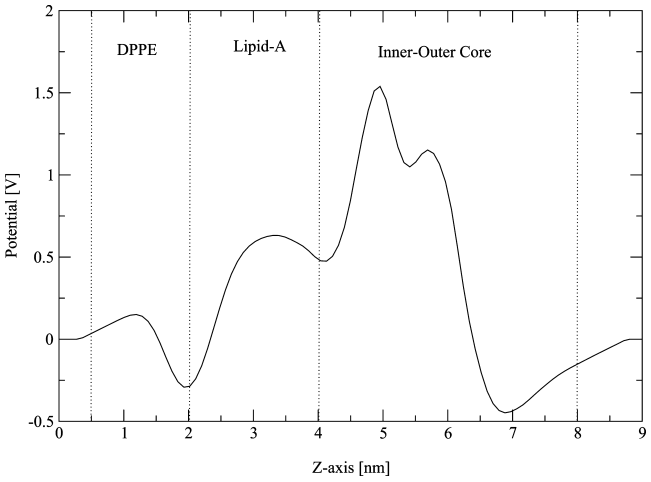

Figure 7. Transmembrane electrostatic potential for the LPS membrane at 350 K. The electrostatic potential calculations were performed using a total of 100 slices and averaged over 32 600 structures saved at 15 ps intervals throughout the last 500 ns of simulations.

5. CONCLUSION

We reported an extension of the GLYCAM06 force field for explicit solvent simulations of LPS membranes. Novel building blocks were added to GLYCAM06 for residues LP1, LP2, PO4, 3H1, 0KO, WLL, XYA, LKO, PH2, and SYB. This parameter set was applied to molecular dynamics simulations of the rough PA01 LPS chemotype from *Pseudomonas aeruginosa* on top of a DPPE monolayer. A total of 1 μs was simulated for a bilayer composed of 72 LPS molecules packed onto 180 DPPE lipids in the liquid crystalline phase at temperatures of 300 and 350 K. The quality of the parameter set was assessed by comparison of calculated properties such as area per lipid molecule, density profiles, and deuterium order parameters against neutron and X-ray diffraction measurements. Our lipopolysaccharide extension of the GLYCAM06 force field reproduced well the experimental area per LPS molecule, the orientational behavior of LPS molecules derived from ATR-FITR spectroscopy, and the high permeability of LPS membranes from *P. aeruginosa* in the liquid-crystalline phase measured by the means of neutron scattering. Remarkably, our simulations show that water molecules can penetrate the hydrocarbon region up to the terminal methyl groups in agreement with the experimental data. The estimated transmembrane potential for the LPS-DPPE bilayer is ca. −119 mV. Therefore, the present parameter set reproduces satisfactorily the overall structure, transmembrane potential, as well as the permeability of LPS membranes in the liquid-crystalline phase.

It has been previously shown that the conformational ensemble and electrostatic properties of the outer membrane F (OprF) from *P. aeruginosa* can differ significantly when simulated in lipid bilayers or their lipopolysaccharide counterparts.[40,42] The extent of these findings has been limited by the short time length of the simulations and the number of outer-membrane proteins investigated so far. The present parameter set together with the associated atomic coordinates and topology files for the equilibrated LPS-DPPE membrane represent a suitable model to further investigate the effect of LPS versus phospholipid membranes on the structural dynamics of outer-membrane proteins in conjunction with the AMBER and GLYCAM force fields.

ASSOCIATED CONTENT

Supporting Information

Dihedral rotational profiles are provided free of charge via the Internet at http://pubs.acs.org. The atomic coordinates of the LPS-DPPE bilayer system and topology files of the LPS molecules can be obtained from the corresponding authors upon request or at the Web site http://dqfnet.ufpe.br/biomat/software.html.

AUTHOR INFORMATION

Corresponding Author

*E-mail: karl.kirschner@scai.fraunhofer.de, thereza.soares@ufpe.br.

Notes

The authors declare no competing financial interest.

ACKNOWLEDGMENTS

This work was partially supported by the Brazilian National Council for Research and Development (CNPq), The State of Pernambuco Research Foundation (FACEPE), INCT-INAMI, nBioNet, Nanobiotec-BR/CAPES, and the Swedish Foundation for International Cooperation in Research and Higher Education (STINT). Computational resources were provided by the Environmental Molecular Sciences Laboratory at Pacific Northwest National Laboratory.

REFERENCES

(1) Erridge, C.; Bennett-Guerrero, E.; Poxton, I. R. *Microbes Infect.* **2002**, *4*, 837−851.
(2) Schindler, M.; Osbron, M. J. *Biochemistry* **1979**, *18*, 4425−4430.
(3) Sadovskaya, I.; Brisson, J. R.; Khieu, N. H.; Mutharia, L. M.; Altman, E. *Eur. J. Biochem.* **1998**, *253*, 319−327.
(4) Wilkinson, S. G. *Prog. Lipid Res.* **1996**, *35*, 283−343.
(5) Lomovskaya, O.; Totrov, M. *J. Bacteriol.* **2005**, *187*, 1879−83.
(6) Nikaido, H. *Semin. Cell Dev. Biol.* **2001**, *12*, 215−23.
(7) Nikaido, H. *Microbiol. Mol. Biol. Rev.* **2003**, *67*, 593−656.
(8) Kumar, A.; Schweizer, H. P. *Adv. Drug. Deliv. Rev.* **2005**, *57*, 1486−513.
(9) Hancock, R. E.; Brinkman, F. S. *Annu. Rev. Microbiol.* **2002**, *56*, 17−38.
(10) Poole, K.; Srikumar, R. *Current Topics in Medicinal Chemistry* **2001**, *1*, 59−71.
(11) Hancock, R. E.; Chapple, D. S. *Antimicrob. Agents Chemother.* **1999**, *43*, 1317−23.
(12) Akama, H.; Kanemaki, M.; Yoshimura, M.; Tsukihara, T.; Kashiwagi, T.; Yoneyama, H.; Narita, S.; Nakagawa, A.; Nakae, T. *J. Biol. Chem.* **2004**, *279*, 52816−9.
(13) Cock, H.; Brandenburg, K.; Wiese, A.; Holst, O.; Seydel, U. *J. Biol. Chem.* **1999**, *271*, 5114−5119.
(14) Hagge, S. O.; Cock, H.; Gutsmann, T.; Beckers, F.; Seydel, U.; Wiese, A. *J. Biol. Chem.* **2001**, *277*, 34247−34253.
(15) Seydel, U.; Eberstein, W.; Schroder, G.; Brandenburg, K. *Z. Naturforsch. C* **1992**, *47*, 757−761.
(16) Pristovsek, P.; Kidric, J. *J. Med. Chem.* **1999**, *42*, 4604−13.
(17) Majerle, A.; Kidric, J.; Jerala, R. *J. Antimicrob. Chemother.* **2003**, *51*, 1159−65.
(18) Bhattacharjya, S. *Curr. Med. Chem.* **2010**, *17*, 3080−93.
(19) Adcock, S. A.; McCammon, J. A. *Chem. Rev.* **2006**, *106*, 1589−615.
(20) Karplus, M.; McCammon, J. A. *Nat. Struct. Biol.* **2002**, *9*, 646−52.
(21) van Gunsteren, W. F.; Bakowies, D.; Baron, R.; Chandrasekhar, I.; Christen, M.; Daura, X.; Gee, P.; Geerke, D. P.; Glattli, A.; Hunenberger, P. H.; Kastenholz, M. A.; Ostenbrink, C.; Schenk, M.; Trzesniak, D.; van der Vegt, N. F. A. *Angewandt. Chem.-Intl Ed.* **2006**, *45*, 4064−4092.

(22) van Gunsteren, W. F.; Bakowies, D.; Burgi, R.; Chandrasekhar, I.; Christen, M.; Daura, X.; Gee, P.; Glattli, A.; Hansson, T.; Oostenbrink, C.; Peter, C.; Pitera, J.; Schuler, L.; Soares, T. A.; Yu, H. B. *Chimia* **2001**, *55*, 856−860.
(23) Feller, S. E.; MacKerell, A. D. *J. Phys. Chem. B* **2000**, *104*, 7510−7515.
(24) Huber, T.; Rajamoorthi, K.; Kurze, V. F.; Beyer, K.; Brown, M. F. *J. Am. Chem. Soc.* **2002**, *124*, 298−309.
(25) Klauda, J. B.; Venable, R. M.; Freites, J. A.; O'Connor, J. W.; Tobias, D. J.; Mondragon-Ramirez, C.; Vorobyov, I.; MacKerell, A. D., Jr.; Pastor, R. W. *J. Phys. Chem. B* **2010**, *114*, 7830−7843.
(26) Sonne, J.; Jensen, M. O.; Hansen, F. Y.; Hemmingsen, L.; Peters, G. H. *Biophys. J.* **2007**, *92*, 4157−67.
(27) Taylor, J.; Whiteford, N. E.; Bradley, G.; Watson, G. W. *Biochim. Biophys. Acta* **2009**, *1788*, 638−649.
(28) Tessier, M. B.; DeMarco, M. L.; Yongye, A. B.; Woods, R. J. 2008, *34*, 349-364.
(29) Chandrasekhar, I.; Kastenholz, M.; Lins, R. D.; Oostenbrink, C.; Schuler, L. D.; Tieleman, D. P.; van Gunsteren, W. F. *Eur. Biophys. J.* **2003**, *32*, 67−77.
(30) Chiu, S. W.; Pandit, S. A.; Scott, H. L.; Jakobsson, E. *J. Phys. Chem. B* **2009**, *113*, 2748−2763.
(31) Griepernau, B.; Leis, S.; Schneider, M. F.; Sikor, M.; Steppich, D.; Bockmann, R. A. *Biochim. Biophys. Acta* **2007**, *1768*, 2899−913.
(32) Poger, D.; Van Gunsteren, W. F.; Mark, A. E. *J. Comput. Chem.* **2010**, *31*, 1117−1125.
(33) Ulmschneider, J. P.; Ulmschneider, M. B. *J. Chem. Theory Comput.* **2009**, *5*, 1803−1813.
(34) Marrink, S. J.; Risselada, H. J.; Yefimov, S.; Tieleman, D. P.; de Vries, A. H. *J. Phys. Chem. B* **2007**, *111*, 7812−7824.
(35) Reynwar, B. J.; Illya, G.; Harmandaris, V. A.; Muller, M. M.; Kremer, K.; Deserno, M. *Nature* **2007**, *447*, 461−464.
(36) Venturoli, M.; Sperotto, M. M.; Kranenburg, M.; Smit, B. *Physical Reports* **2006**, *437*, 1−54.
(37) Lins, R. D.; Vorpagel, E. R.; Guglielmi, M.; Straatsma, T. P. *Biomacromolecules* **2008**, *9*, 29−35.
(38) Lins, R. D.; Straatsma, T. P. *Biophys. J.* **2001**, *81*, 1037−1046.
(39) Soares, T. A.; Lins, R. D.; Straatsma, T. P. *J. Braz. Chem. Soc.* **2008**, *19*, 312−320.
(40) Soares, T. A.; Straatsma, T. P. *AIP Conf. Proc.* **2007**, *963*, 1375−1378.
(41) Soares, T. A.; Straatsma, T. P. *Mol. Simul.* **2008**, *34*, 295−307.
(42) Straatsma, T. P.; Soares, T. A. *Proteins: Struct., Funct., Genet.* **2009**, *74*, 475−488.
(43) Moraru, A.; Svab, I.; Mihailescu, D. F. *Revue Roumaine de Chimie* **2009**, *54*, 799−805.
(44) Cornell, W.; Cieplak, P.; Bayly, C.; Gould, I.; Merz, K.; Ferguson, D.; Spellmeyer, D.; Fox, T.; Caldwell, J.; Kollman, P. *J. Am. Chem. Soc.* **1995**, *117*, 5179−5197.
(45) Woods, R. J.; Dwek, R. A.; Edge, C. J.; Fraser-Reid, B. *J. Phys. Chem.* **1995**, *99*, 3832−3846.
(46) Pontes, F. J. S.; Rusu, V. H.; Soares, T. A.; Lins, R. D. *J. Chem. Theory Comput.* **2012**, DOI: 10.1021/ct300084v.
(47) Piggot, T. J.; Holdbrook, D. A.; Khalid, S. *J. Phys. Chem. B* **2011**, *115*, 13381−13388.
(48) Kirschner, K. N.; Yongye, A. B.; Tschampel, S. M.; Gonzalez-Outeirino, J.; Daniels, C. R.; Foley, B. L.; Woods, R. J. *J. Comput. Chem.* **2008**, *29*, 622−655.
(49) Lange, O. F.; van der Spoel, D.; de Groot, B. L. *Biophys. J.* **2010**, *99*, 647−655.
(50) Oostenbrink, C.; Soares, T. A.; van der Vegt, N. F.; van Gunsteren, W. F. *Eur. Biophys. J.* **2005**, *34*, 273−824.
(51) Soares, T. A.; Daura, X.; Oostenbrink, C.; Smith, L. J.; van Gunsteren, W. F. *J. Biomol. NMR* **2004**, *30*, 407−422.
(52) van Gunsteren, W. F.; Mark, A. E. *J. Phys. Chem.* **1998**, *108*, 6109−6116.
(53) Cornell, W. D.; Cieplak, P.; Bayly, C. I.; Gould, I. R.; Merz, K. M.; Ferguson, D. M.; Spellmeyer, D. C.; Fox, T.; Caldwell, J. W.; Kollman, P. A. *J. Am. Chem. Soc.* **1995**, *117*, 5179−5197.
(54) Lins, R. D.; Hunenberger, P. H. *J. Comput. Chem.* **2005**, *26*, 1400−1412.
(55) Schmid, N.; Eichenberger, A. P.; Choutko, A.; Riniker, S.; Winger, M.; Mark, A. E.; van Gunsteren, W. F. *Eur Biophys J* **2011**, *40*, 843−56.
(56) Gandhi, N. S.; Mancera, R. L. *Carbohydr. Res.* **2010**, *30*, 689−695.
(57) Sattelle, B. M.; Bose-Basu, B.; Tessier, M.; Woods, R. J.; Serianni, A. S.; Almond, A. *J. Phys. Chem. B* **2012**, *116*, 6380−6386.
(58) Taha, H. A.; Roy, P.-R.; Lowary, T. L. *J. Chem. Theory Comput.* **2011**, *7*, 420−432.
(59) Schrodinger, LLC, The Pymol Molecular Graphics System, Version 1.3r1. In 2010.
(60) Schmidt, M. W.; Baldridge, K. K.; Boatz, J. A.; Elbert, S. T.; Gordon, M. S.; Jensen, J. H.; Koseki, S.; Matsunaga, N.; Nguyen, K. A.; Su, S.; Windus, T. L.; Dupuis, M.; Montgomery, J. A. *J. Comput. Chem.* **1993**, *14*, 1347−1363.
(61) Guha, R.; Howard, M. T.; Hutchison, G. R.; Murray-Rust, P.; Rzepa, H.; Steinbeck, C.; Wegner, J.; Willighagen, E. L. *J. Chem. Inf. Model.* **2006**, *46*, 991−998.
(62) Bayly, C. I.; Cieplak, P.; Cornell, W.; Kollman, P. A. *J. Phys. Chem.* **1993**, *97*, 10269−10280.
(63) Breneman, C. M.; Wiberg, K. B. *J. Comput. Chem.* **1990**, *11*, 361−373.
(64) Woods, J. R.; Khalil, M.; Pell, W.; Moffat, H. S.; Smith, H. V. *J. Comput. Chem.* **1990**, *11*, 297−310.
(65) Dupradeau, F. Y.; Pigache, A.; Zaffran, T.; Savineau, C.; Lelong, R.; Grivel, N.; Lelong, D.; Rosanski, W.; Cieplak, P. *Phys. Chem. Chem. Phys.* **2010**, *12*, 7821−7839.
(66) Case, D. A.; Cheatham, T. E., 3rd; Darden, T.; Gohlke, H.; Luo, R.; Merz, K. M., Jr.; Onufriev, A.; Simmerling, C.; Wang, B.; Woods, R. J. *J. Comput. Chem.* **2005**, *26*, 1668−1688.
(67) *Amber09*, University of California: San Francisco, CA: 2006.
(68) van der Spoel, D.; Lindahl, E.; Hess, B.; Groenhof, G.; Mark, A. E.; Berendsen, H. J. C. *J. Comput. Chem.* **2005**, *26*, 1701−1718.
(69) Reith, D.; Kirschner, K. N. *Comput. Phys. Commun.* **2011**, *182*, 2184−2191.
(70) *Gnuplot 4.5: An Interactive Plotting Program*, 2011.
(71) Sadovskaya, I.; Brisson, J. R.; Lam, J. S.; Richards, J. C.; Altman, E. *Eur. J. Biochem.* **1998**, *255*, 673−684.
(72) Sadovskaya, I.; Brisson, J. R.; Thibault, P.; Richards, J. C.; Lam, J. S.; Altman, E. *Eur. J. Biochem.* **2000**, *267*, 1640−1650.
(73) Snyder, S.; Kim, D.; McIntosh, T. J. *Biochemistry* **1999**, *38*, 10758−10767.
(74) Abraham, T.; Schooling, S. R.; Nieh, M. P.; Kucerka, N.; Beveridge, T. J.; Katsaras, J. *J. Phys. Chem. B* **2007**, *111*, 2477−2483.
(75) Brandenburg, K.; Andra, J.; Muller, M.; Koch, M. H.; Garidel, P. *Carbohydr. Res.* **2003**, *338*, 2477−89.
(76) Jorgensen, W. L.; Chandrasekhar, J.; Madura, J. D.; Impey, R. W.; Klein, M. L. *J. Chem. Phys.* **1983**, *79*, 926−936.
(77) Berendsen, H. J. C.; Postma, J. P. M.; DiNola, A.; Haak, J. R. *J. Chem. Phys.* **1984**, *81*, 3684−3691.
(78) Hess, B. *J. Chem. Theory Comput.* **2007**, *4*, 116−122.
(79) Tironi, I. G.; Sperb, R.; Smith, P. E.; van Gunsteren, W. F. *J. Chem. Phys.* **1995**, *102*, 5451−5459.
(80) Hess, B., Kutzner, C., van der Spoel, D., Lindahl, E. *J. Chem. Theory Comput.* 2008, *4*.
(81) Humphrey, W.; Dalke, A.; Schulten, K. *J. Mol. Graphics* **1996**, *14*, 33−38.
(82) Thurmond, R. L.; Dodd, S. W.; Brown, M. F. *Biophys. J.* **1991**, *59*, 108−113.
(83) Leekumjorn, S.; Sum, A. K. *Biophys. J.* **2006**, *90*, 3951−3965.
(84) Kucerka, N.; Papp-Szabo, E.; Nieh, M. P.; Harroun, T. A.; Schooling, S. R.; Pencer, J.; Nicholson, E. A.; Beveridge, T. J.; Katsaras, J. *J. Phys. Chem. B* **2008**, *112*, 8057−8062.
(85) Nagle, J. F.; Tristram-Nagle, S. *Biochim. Biophys. Acta* **2000**, *1469*, 159−195.
(86) Brandenburg, K.; Mayer, H.; Koch, M. H.; Weckesser, J.; Rietschel, E. T.; Seydel, U. *Eur. J. Biochem.* **1993**, *218*, 555−563.

(87) Brandenburg, K.; Seydel, U. *Eur. J. Biochem.* **1988**, *16*, 83−94.
(88) Brandenburg, K.; Seydel, U. *Eur. J. Biochem.* **1990**, *191*, 229−236.
(89) Tamm, L. K.; Tatulian, S. A. *Q. Rev. Biophys.* **1997**, *30*, 365−429.
(90) Brandenburg, K. *Biophys. J.* **1993**, *64*, 1215−1231.
(91) Brandenburg, K.; Funari, S. S.; Koch, M. H.; Seydel, U. *J. Struct. Biol.* **1999**, *128*, 175−186.
(92) Wiese, A.; Reiners, J. O.; Brandenburg, K.; Kawahara, K.; Zahringer, U.; Seydel, U. *Biophys. J.* **1996**, *70*, 321−329.
(93) Gurtovenko, A. A.; Vattulainen, I. *J. Am. Chem. Soc.* **2007**, *129*, 5358−5359.
(94) Lee, S. J.; Song, Y.; Baker, N. A. *Biophys. J.* **2008**, *94*, 3565−3576.
(95) Latorre, R.; Hall, J. E. *Nature* **1976**, *264*, 361−363.
(96) White, D. A.; Lennarz, W. J.; Schnaitman, C. A. *J. Bacteriol.* **1972**, *109*, 686−690.
(97) Ishinaga, M.; Kanamoto, R.; Kito, M. *J. Biochem.* **1979**, *86*, 161−165.
(98) The GLYCAM Force Field. 2012. http://glycam.ccrc.uga.edu/ccrc/pages/parameters.html (Acessed Aug. 20, 2012)